Scientific Reports

https://doi.org/10.1038/s41598-026-46881-4

Article in Press

Marine bacterium *Stutzerimonas stutzeri* mitigates Parkinson's disease pathology in *C. elegans* via ferroptosis modulation

Received: 26 November 2025

Accepted: 27 March 2026

Published online: 03 April 2026

Cite this article as: Singh S., Damodaran A., Goswami S. *et al.* Marine bacterium *Stutzerimonas stutzeri* mitigates Parkinson's disease pathology in *C. elegans* via ferroptosis modulation. *Sci Rep* (2026). https://doi.org/10.1038/s41598-026-46881-4

Simran Singh, Anusree Damodaran, Sanskriti Goswami, Manjul Lata, Mukesh Pasupuleti & Sonia Verma

Title

Marine Bacterium *Stutzerimonas stutzeri* Mitigates Parkinson's disease Pathology in *C. elegans* via Ferroptosis Modulation

Author names

Simran Singh[a, c,*], Anusree Damodaran[a], Sanskriti Goswami[a], Manjul Lata[b, c], Mukesh Pasupuleti[b, c], Sonia Verma[a, c#]

Affiliations

[a]Division of Neuroscience and Ageing Biology, CSIR-Central Drug Research Institute, Lucknow, UP, India;

[b]Division of Molecular Microbiology & Immunology, CSIR-Central Drug Research Institute, Lucknow, UP, India;

[c] Academy of Scientific and Innovative Research (AcSIR), Ghaziabad 201002, India

*First Author

[#]Corresponding Author

Sonia Verma

Email Address- sonia.verma1@cdri.res.in

Full postal address- Sonia Verma, Senior Scientist, Division of Neuroscience and Ageing Biology, CSIR-Central Drug Research Institute, Lucknow, UP, India.

Abstract

Parkinson's disease (PD) is a rapidly escalating neurodegenerative disorder marked by dopaminergic neurodegeneration, α-synuclein aggregation, and motor and non-motor impairments. Current therapies largely provide symptomatic relief and fail to prevent disease progression, underscoring the need for novel disease-modifying strategies. The marine biome has emerged as an unexplored reservoir of bioactive metabolites with neuroprotective potential, yet their therapeutic relevance in PD remains incompletely explored. Here, we report that *Stutzerimonas stutzeri*, a marine bacterium isolated from the Gulf of Mannar, exerts robust neuroprotective effects in *Caenorhabditis elegans* PD models. Dietary administration of *S. stutzeri* rescued dopaminergic neuronal loss, mitigated α-synuclein expression, and improved motor and sensory phenotypes. Mechanistic analyses revealed suppression of ferroptosis, evidenced by restoration of iron homeostasis, attenuation of lipid peroxidation, and recovery of *ftn-1* expression. Our findings establish *S. stutzeri* as a previously unrecognized marine-derived therapeutic prospect for PD intervention and highlight ferroptosis modulation as a tractable therapeutic axis in neurodegeneration.

1. Introduction

Parkinson's disease (PD) is one of the fastest-growing neurological disorders, with prevalence projected to exceed 12 million cases by 2040 [1,2]. Its core clinical features arise from dopaminergic (DA) neurodegeneration in the substantia nigra pars compacta (SNpc), manifesting as tremor, rigidity, and bradykinesia. Non-motor symptoms such as cognitive decline, autonomic dysfunction, depression, and hyposmia further exacerbate disease burden [3]. Existing therapeutic modalities, including dopamine agonists and monoamine oxidase B inhibitors, though they offer symptomatic relief, often fall short of efficacy and are accompanied by a spectrum of side effects [4,5]. Thus, exploring alternative approaches beyond symptom management and targeting underlying disease mechanisms is crucial. In this context, identifying and developing novel therapeutics holds immense promise for disease modification and improved clinical outcomes in PD.

Ferroptosis is a regulated, iron-dependent form of cell death distinct from apoptosis and necroptosis, first described by Dixon et al. in 2012. It is characterized by lipid peroxidation and has been implicated in several diseases, including neurodegeneration [6,7]. In PD, elevated iron levels, increased lipid peroxidation, and reduced glutathione support a role for ferroptosis in DA neuron loss [8-12]. Notably, the ferroptosis inhibitor ferrostatin-1 has been shown to preserve DA neurons and improve behavioral outcomes in neurotoxin-induced PD models [13]. Additional evidence from other *in vivo* and *in vitro* PD models further reinforces the involvement of ferroptosis. These findings underscore the therapeutic potential of targeting ferroptosis in PD [14-16].

Model organisms are widely used to search for new therapies for PD because they share many similarities with human biology, including the molecular and cellular mechanisms involved in the disease. *Caenorhabditis elegans* is the model organism of choice for investigating the genetics of aging and neurodegeneration owing to its short lifespan and homology in its genetic makeup with humans [17,18]. The available genetic *C. elegans* PD models display multiple phenotypic deficits, including age-dependent aggregation, the loss of DA neurons, and disruption of DA-dependent behaviors. These models have uncovered various genetic factors and chemical compounds that attenuate DA neurodegeneration [17,18]. Thus, using these models can help successfully test the efficacy of and uncover new therapies based on marine bacteria for PD with the potential to translate to humans.

Over the past two decades, the marine environment has emerged as a rich source of bioactive compounds with therapeutic potential, including applications in PD. More than 50 molecules from marine bacteria, fungi, seaweeds, and other organisms have shown promise in preclinical or clinical studies [19,20]. For example, NP7 from *Streptomyces* species crosses the blood–brain barrier, prevents oxidative stress-induced neuronal death, and inhibits microglial

activation [21,22]. Similarly, piloquinones A and B from *Streptomyces* sp. CNQ-027 acts as a potent monoamine oxidase-B inhibitor, a validated PD drug target [21,23]. Several marine-derived metabolites have also advanced to clinical trials: docosahexaenoic acid alleviated depressive symptoms in PD patients (NCT01563913), inosine increased serum and CSF urate levels as a potential disease-modifying agent (NCT02642393), and ganglioside GM1 showed early symptomatic benefits (NCT00037830) [24]. These findings underscore the marine biome as an underexplored reservoir for developing innovative neuroprotective therapies in PD.

Here, we investigated the neuroprotective potential of *Stutzerimonas stutzeri*, a marine bacterium isolated from the sea samples collected from the Gulf of Mannar region, India. *S. stutzeri* was identified from an initial screen of marine bacterial isolates for neuroprotective activity in *C. elegans* models of PD and was selected for further mechanistic investigation based on its consistent protective effects. While previously studied for environmental applications, its therapeutic properties remain unexplored [25,26]. We used transgenic *C. elegans* PD models to show that dietary administration of *S. stutzeri* rescues DA neurodegeneration, reduces α-synuclein burden, and improves motor and sensory functions. Mechanistically, these effects were linked to the suppression of ferroptosis, as evidenced by restoration of *ftn-1* expression, reduced lipid peroxidation, and normalized iron homeostasis. These findings identify *S. stutzeri* as a novel marine bacterium with therapeutic potential and highlight ferroptosis as a tractable target for developing neuroprotective strategies in PD (**Graphical Abstract**).

2. Materials and Methods

2.1. Isolation of *Stutzerimonas. stutzeri*

S. stutzeri, a marine bacterium isolated from the Gulf of Mannar, was previously collected as part of routine explorative work [27]. Briefly, a seawater sample was collected from the Gulf of Mannar in transport media (g/L NaCl 28.32; $MgCl_2$ 5.14; $CaCl_2$ 1.14; KCl 0.69; KBr 0.1; H_3BO_3 0.027; $SrCl_2$ 0.026; NH_4Cl 0.0064; NaF 0.003; $NaSiO_3$ 0.002; $FePO_4$ 0.001; Yeast extract or beef extract 1.0). Serial dilutions of the collected samples were spread on Zobell's marine growth medium and incubated at 37°C for two days. Colonies of different morphology had been isolated and subjected to bacterial identification through 16S rRNA gene amplification [27].

Genomic DNA was isolated from marine bacteria using GenElute Bacterial genomic DNA kit mini, Sigma, Catalogue No. NA2110, and 16S rRNA gene amplification was done using the set of primers, 27F and 1387R, and 63F and 1525R as reported elsewhere [27]. The sequence of these primers is provided in **Table 1**. The obtained amplicon was submitted for DNA sequencing using an ABI 3730 XL sequencer. The obtained sample was then checked for contigs and inconsistency among the readout of the sample with the help of the web-based tool DECIPHER and DNA Baser [28,29]. The final processed 16S rRNA sequencing data were then used for blast analysis. The partial sequence of the 16S rRNA gene results obtained from the Standard Nucleotide Blast analysis were submitted to the NCBI accession number (NCBI GenBank: PQ817733.1).

2.2. Maintenance of *C. elegans* strains

The following transgenic *C. elegans* strains were used in this study:

UA44 [baInl1 (P_{dat-1}::αsyn, P_{dat-1}::GFP)] – expresses human α-synuclein and GFP in DA neurons under the *dat-1* promoter. This strain exhibits age-dependent DA neurodegeneration and reduced dopamine-dependent behaviors.

BY250 vtIs7 [P_{dat-1}::GFP] – expresses GFP under the DA neuron–specific *dat-1* promoter, allowing visualization of DA neuron integrity. Worms display intact DA neurons and serve as a healthy control strain for UA44.

NL5901 [P_{unc-54}::α-synuclein::YFP + unc-119(+)] – expresses human α-synuclein fused to YFP in body-wall muscle cells under the *unc-54* promoter. This strain develops visible α-synuclein aggregates with age, enabling quantification of aggregation burden.

The UA44 strain was kindly gifted by Dr. Anoopkumar Thekkuveettil (Sree Chitra Tirunal Institute for Medical Sciences and Technology, Thiruvananthapuram, Kerala, India). Other *C. elegans* strains were obtained from the *Caenorhabditis* Genetics Center (University of

Minnesota, USA) and maintained on nematode growth medium (NGM) plates seeded with *Escherichia coli* OP50 at 20°C [30]. To obtain synchronized populations, adult worms were bleached to isolate eggs hatched in M9 buffer and arrested at the first larval (L1) stage after 16–18 h at 20°C [30]. Age-synchronized L1 larvae were then transferred to experimental NGM plates seeded with either OP50 or *S. stutzeri*.

All phenotypic, behavioral, and molecular analyses were conducted on Day 3 of adulthood, with the identical feeding regimen applied across all experiments. Day 3 of adulthood was selected because DA neurodegeneration and α-synuclein–associated phenotypes are robustly detectable at this stage in established *C. elegans* models of PD [31].

2.3. Preparation of bacteria-seeded NGM plates

Both *E. coli* OP50 and *S. stutzeri* were cultured overnight at 37°C under strain-specific conditions, with OP50 grown in Luria–Bertani broth (GLR Innovations, Cat. No. GLRCM0054) and *S. stutzeri* in Zobell's Marine Broth (HiMedia, Cat. No. M385-500G). Following incubation, bacterial cells were pelleted by centrifugation at 6000 rpm, washed thrice with M9 buffer, and resuspended in the same buffer to a 2 mg/mL concentration. A 0.5 mL aliquot of this suspension was spread on 60 mm NGM plates, which were left in a laminar hood for 16 h before putting L1-stage worms. To suppress progeny development, fluoro-2′-deoxy-β-uridine (TCI, Cat. No. D2235) was added at a 0.1 mg/mL concentration at the fourth larval stage [32]. Worms at day three of adulthood were used for subsequent assessments. Under the experimental conditions used, *S. stutzeri* formed stable bacterial lawns, and worms exhibited normal feeding behavior without overt aversion or gross phenotypic abnormalities compared with OP50-fed controls.

2.4. Assessment of DA neuronal health

The degeneration of DA neurons was assessed on Day 3 of adulthood by analysing the fluorescence images of UA44 and BY250 [33]. Worms were collected from culture plates, washed with M9 buffer, and mounted on 2% agarose pads prepared on glass slides. Animals were anesthetized with 30 mM sodium azide (Sigma, Cat. No. S2002) and covered with a coverslip. Fluorescence images of the head region were acquired at 20× magnification using a Leica DMi6000 microscope. Images were quantified through ImageJ software by closely selecting DA neurons of the head region of worms (ImageJ, National Institutes of Health, Bethesda, MD). A minimum of 40 worms (pooled from at least three independent biological replicates) were imaged for each experiment condition.

2.5. Assessment of α-synuclein expression

Alpha-synuclein expression was assessed on Day 3 of adulthood by analysing the fluorescence images of NL5901 [34]. Worms were collected, washed with M9 buffer, and mounted on 2% agarose pads prepared on glass slides. Worms were anesthetized using 30 mM sodium azide and immobilized under a coverslip. Fluorescence images were captured at 10x magnification with a Leica DMi6000 fluorescence microscope. Quantification of fluorescence intensity was subsequently performed using ImageJ software. A minimum of 40 worms (pooled from at least three independent biological replicates) were imaged per experimental condition.

2.6. Quantification of pharyngeal pumping rate

The pharyngeal pumping rate was quantified on Day 3 of adulthood following the established protocol [35]. Briefly, a minimum 30-second video was recorded for each worm under a dissection microscope (Weswox Optik SZM-102) fitted with a camera. Pharyngeal contractions were manually counted over 30 seconds to determine the pumping rate. For each experimental condition, at least 40 worms (pooled from at least three independent biological replicates) were analyzed.

2.7. Nonanol repulsion assay

The nonanol repulsion assay was conducted on Day 3 of adulthood to evaluate avoidance behavior in *C. elegans* following a modified version of established protocols [36,37]. Worms were thoroughly washed with M9 buffer, and at least 30 worms were transferred to the centre of 60 mm unseeded NGM plates divided into four quadrants. A 1 µL drop of 1-nonanol (TCI, Cat. No. N0292) was placed on diagonally opposite quadrants. After 45-minute incubation at 20 °C, worms were counted in each quadrant, and a repulsion index was calculated using the formula:

$$\text{Repulsion Index} = \frac{\text{Number of worms (Nonanol quadrant - Non-Nonanol Quadrant)}}{\text{Total Number of worms}}$$

The assay was repeated with at least three independent biological replicates.

2.8. RNA isolation and quantitative real-time PCR (qRT-PCR)

On Day 3 of adulthood, worms were collected, washed with M9 buffer, and homogenized in Trizol (Sigma-Aldrich, T9424-200ML) reagent through repeated freeze-thaw cycles and vortexing. Total RNA was extracted using phenol:chloroform: isoamyl alcohol separation followed by isopropanol precipitation, and approximately 2 µg of purified RNA was reverse-transcribed into cDNA using GoScript Reverse Transcription System (Promega, Cat. No. A5001) [35]. qRT-PCR was performed using SYBR Premix Ex Taq (TaKaRa Bio Inc., Cat. No. RR420A) and RT-PCR machine (Biorad-CFX96), with *β-actin* serving as the internal control for

normalization. Gene expression was analyzed using the $2^{-\Delta\Delta Ct}$ method [35]. The sequences of all primers used in this study are given in **Table 1**.

2.9. BODIPY staining

BODIPY 581/591 (Invitrogen, Cat. No. D3861) is a lipid peroxidation–sensitive dye that emits red fluorescence in its reduced (non-oxidized) state and shifts to green fluorescence upon oxidation. Therefore, lipid peroxidation was quantified by calculating the ratio of green (oxidized) to red (non-oxidized) fluorescence intensity. BODIPY staining was performed on Day 3 of adulthood following established protocols to assess lipid distribution in *C. elegans* [38]. A 5 mg/ml BODIPY stock solution was prepared in DMSO and diluted to a 1 µg/ml working concentration in M9 buffer. On Day 3 of adulthood, worms were collected, washed, and incubated with 500 µl of the staining solution for 90 min at room temperature with gentle rotation. Post-incubation, worms were washed and mounted on slides. Fluorescence images were captured at 10x magnification with a Leica DMi6000 fluorescence microscope. Quantification of fluorescence was carried out using ImageJ software. A minimum of 40 worms (pooled from at least three independent biological replicates) were imaged per experimental condition.

2.10. Malondialdehyde (MDA) assay

MDA levels were measured on Day 3 of adulthood using the MDA Colorimetric Assay Kit (Elabsciences, Cat. No. E-BC-K025-S) according to the manufacturer's instructions. Briefly, protein extracts prepared from worm pellets were reacted with clarificant, acid reagent, and chromogenic solution, while control reactions replaced the chromogenic solution with 50% glacial acetic acid. Samples were incubated at 95°C for 2 h in a water bath and then rapidly cooled under running water to stabilize the reaction products. The absorbance of the resulting mixtures was recorded at 532 nm, and MDA concentrations were quantified using the standard formula provided in the kit protocol. The assay was repeated with at least three independent biological replicates.

2.11. Tissue iron content assay

Total iron concentrations were quantified on Day 3 of adulthood using the Tissue Iron Content Assay Kit (RealGene, Cat. No. 250435) according to the manufacturer's protocol. Briefly, worm pellets were homogenized in the provided extraction buffer by sonication and centrifuged at 4000 × g. The resulting lysates were incubated with the provided reagents and standards, heated briefly in a boiling water bath, and rapidly cooled. The aqueous phase was collected for analysis after chloroform extraction and high-speed centrifugation at 10,000 rpm. Absorbance was measured at 520 nm, and iron levels were calculated based on the kit's

specified formula. The assay was repeated with at least three independent biological replicates.

2.12. Transcriptomic analysis

For each condition (UA44 fed on either OP50 or *S. stutzeri*), worms were cultured in six independent biological replicates, with approximately 500 worms per replicate. On the third day of adulthood, three replicates were pooled, generating two pooled biological samples (>1500 worms each) per condition [39-42]. Worm pellets were washed, snap-frozen, and processed at Biokart Genomics Lab (Bengaluru, India) for RNA isolation, sequencing, and analysis. Briefly, total RNA was extracted using the RNeasy Mini Kit (Qiagen), and integrity was verified (RNA Integrity Number > 7.0). Libraries were prepared with the NEBNext Ultra II RNA Library Prep Kit and sequenced on an Illumina HiSeq platform to obtain paired-end reads. RNA-Seq data was analyzed using the Galaxy platform [43]. Quality assessment (FastQC) and trimming (Trimmomatic) were followed by alignment to the *C. elegans* ce11 genome (HISAT2) and quantification (featureCounts). Differential expression analysis was conducted using the LIMMA package after voom normalization. Genes with an adjusted $p \leq 0.05$ and |log2 fold-change| ≥ 0.5 were considered significantly differentially expressed.

2.13. Functional enrichment analysis

Functional enrichment analysis of Gene Ontology (GO) terms was performed using the Database for Annotation, Visualization, and Integrated Discovery (DAVID) (https://david.ncifcrf.gov/) [44]. Enriched functional categories were defined as GO terms or Reactome pathways with statistical significance at $p \leq 0.05$. The GO analysis encompassed biological processes, cellular components, and molecular functions, thereby characterizing the activities and subcellular localization of the associated genes. Visualization of enriched GO terms and Reactome pathways was conducted in RStudio (version 1.3.959; https://rstudio.com/) using the ggplot2 package to generate bubble plots [45].

2.14. Statistical analysis

Statistical analyses were performed using GraphPad Prism version 8.0 (GraphPad Software, La Jolla, CA, USA). Data are presented as mean ± standard deviation. Comparisons between groups were conducted using Student's t-test, and differences were considered statistically significant at $p \leq 0.05$.

3. Results

3.1. 16S rRNA sequencing confirms the identity of the isolate as *S. stutzeri*

The first objective was to identify the bacteria to avoid redundancy and repetition of the work. So we have performed the PCR amplification and sequencing of the 16S rRNA gene with the help of universal 16S rRNA primer sets. The obtained 1.5 kb long amplicon sequence was checked for contigs and inconsistencies to remove the low readout bases from the sequence and enhance the quality of the sequence. The blast analysis results of the final processed 16S rRNA sequencing data was then used for Standard Nucleotide blast analysis using 16S ribosomal RNA (Bacteria and Archaea type strains), and other default settings showed that the isolated bacterium is *Stutzerimonas stutzeri* (**Supplementary Information 1**).

Recent advances in whole genome sequencing techniques have indicated that *Stutzerimonas* is a new genus with some similarity to that of *Pseudomonadaceae* [46]*. Stutzerimonas stutzeri* has earlier been reported as a Gram-negative, facultative anaerobic bacterium with natural denitrification ability [47].

3.2. *S. stutzeri* prevents DA neurodegeneration in UA44

PD pathology in humans is defined by progressive degeneration of DA neurons in the SNpc [48]. To model this hallmark feature in *C. elegans*, we examined DA neuron integrity using fluorescence microscopy on day three of adulthood. As expected, UA44 (OP50) (24.89 ± 1.05) worms exhibited a significant reduction in DA neuron fluorescence compared to the control strain BY250 (OP50) (42.31 ± 1.48; $p < 0.0001$), confirming the degenerative phenotype. Strikingly, UA44 (*S. stutzeri*) (35.58 ± 0.96; $p < 0.0001$) displayed a significant prevention of DA neuron fluorescence intensity relative to UA44 (OP50), indicating that *S. stutzeri* exerts a neuroprotective effect on DA neurons and mitigates PD-like pathology (**Figure 1A and 1B**).

To exclude potential developmental confounding, we assessed developmental rate in BY250 (OP50), UA44 (OP50), and UA44 (*S. stutzeri*). No significant differences were observed between the two conditions (**Supplementary Information 2**).

3.3. *S. stutzeri* prevents neuro-sensory and motor deficits in UA44

After establishing DA neuroprotection, we assessed whether *S. stutzeri* influences dopamine-dependent behaviour on Day 3 of adulthood. Dopamine regulates multiple processes in *C. elegans*, including motivation, memory, and motor control, and changes in dopamine levels alter responses to attractants and repellents [49,50]. We used the well-established 1-nonanol repellent assay to indirectly estimate dopamine function, where

normal dopamine promotes robust avoidance, while reduced dopamine delays repulsion [51,52]. In the 1-nonanol repellent assay, UA44 (OP50) worms (-0.14 ± 0.04) exhibited a significantly reduced aversive response compared to BY250 (OP50) (-0.66 ± 0.03; $p < 0.0001$), consistent with impaired dopamine signalling. Importantly, UA44 (*S. stutzeri*) worms (-0.72 ± 0.04; $p < 0.0001$) displayed a significant improvement in repulsion index relative to UA44 (OP50), indicating preservation of dopamine-associated chemotaxis (**Figure 2A**).

To further evaluate motor function, we measured pharyngeal pumping, a rhythmic neuromuscular behavior that reflects both neural and muscle health [53,54]. Increased expression-dependent aggregation of α-synuclein is known to suppress this behavior. Consistent with this, UA44 (OP50) worms (52.50 ± 2.09) exhibited a significant reduction in pumping rate compared to BY250 (OP50) (86.60 ± 3.37; $p < 0.0001$), validating the neuromuscular deficit in the PD model. Remarkably, UA44 (*S. stutzeri*) worms (79.40 ± 3.19; $p < 0.0001$) retained significantly higher pharyngeal pumping rates than UA44 (OP50), demonstrating a protective effect of *S. stutzeri* against α-synuclein-induced dysfunction (**Figure 2B)**.

3.4. *S. stutzeri* limits α-synuclein expression in NL5901

Elevated α-synuclein is a central driver of neurodegeneration in mammalian and *C. elegans* models of PD [55]. To determine whether *S. stutzeri* modulates α-synuclein pathology, we employed the NL5901 transgenic strain. on Day 3 of adulthood, NL5901 (OP50) worms exhibited pronounced α-synuclein expression, evident as increased punctate fluorescence (86.14 ± 4.44), confirming the aggregation-prone phenotype. By contrast, NL5901 (*S. stutzeri*) (71.83 ± 3.09; $p < 0.01$) displayed a significant reduction in fluorescence intensity relative to NL5901 (OP50), indicating suppression of α-synuclein accumulation (**Figure 3A and 3B**).

To dissect this effect, we quantified α-synuclein mRNA levels. NL5901 (*S. stutzeri*) worms showed a significant decrease in α-synuclein transcript (0.20 ± 0.20; $p < 0.05$) relative to NL5901 (OP50) (**Figure 3C**). This reduction suggests that *S. stutzeri* likely acts at the transcriptional level, at least in part, thereby limiting α-synuclein mRNA availability and downstream protein accumulation.

3.5. *S. stutzeri* drives global transcriptomic modulation

Given the protective effects of *S. stutzeri* on DA neurons, behavior, and α-synuclein expression, we next compared the transcriptomic profiles of UA44 (OP50) and UA44 (*S. stutzeri*) on Day 3 of adulthood. This analysis identified 11,950 differentially expressed genes (DEGs) ($p \leq 0.05$, $|\log2 \text{ fold-change}| \geq 0.5$), including 5,812 upregulated and 6,138

downregulated transcripts in the *S. stutzeri* group (**Figure 4A and 4B**). A heatmap of the top 50 DEGs revealed clear segregation between the two conditions, highlighting distinct transcriptional signatures (**Figure 4C**). These results demonstrate that *S. stutzeri* induces widespread transcriptomic reprogramming in the UA44 PD model, providing a foundation for pathway-level analyses to uncover mechanisms underlying its neuroprotective effects.

3.6. Functional and pathway analysis of DEGs links transcriptional changes to iron homeostasis

We performed comprehensive GO and pathway enrichment analyses to explore the functional significance of the 11,950 DEGs. GO analysis identified the top five significantly enriched biological processes, which included proteolysis, protein dephosphorylation, locomotion, protein transmembrane transport, and response to heat (**Figure 5A and Supplementary Information 3**). The top five significantly enriched molecular functions involved protein binding, ATP binding/hydrolysis, cuticle structural constituents, and metallopeptidase activity (**Figure 5B and Supplementary Information 3**). The most significantly enriched cellular components included cytoplasm, nucleus, mitochondria, cytosol, and extracellular region (**Figure 5C and Supplementary Information 3)**. Reactome pathway analysis further revealed enrichment of neutrophil degranulation, metabolism, aerobic respiration, respiratory electron transport, nucleotide excision repair, and iron uptake/transport pathways (**Figure 5D and Supplementary Information 3**). These results indicate that the DEGs are functionally linked to proteostasis, energy metabolism, and iron homeostasis, highlighting pathways relevant to neurodegeneration and PD pathology.

3.7. *S. stutzeri* protects against ferroptosis in UA44 worms

Reactome pathway analysis of DEGs highlighted the dysregulation of the iron uptake and transport pathway, a process closely associated with ferroptosis, an iron-dependent form of regulated cell death. Aberrant iron accumulation in the SNpc and ferroptosis-related oxidative damage have been consistently reported in PD patients, positioning ferroptosis as a mechanistic driver of DA neurodegeneration and leading us to hypothesize that *S. stutzeri* may confer neuroprotection by modulating ferroptosis [56,57]. In our transcriptomic dataset, the *C. elegans* ortholog of the gene coding for ferritin heavy chain, *ftn-1*, was significantly downregulated in UA44 (*S. stutzeri*) ($\log_2$ fold-change= -2.88; p <0.01) compared to UA44 (OP50) (**Figure 6A**). This finding was independently validated by qRT-PCR, which confirmed reduced *ftn-1* expression in UA44 (*S. stutzeri*) (0.26 ± 0.14; p < 0.01) (**Figure 6B**). This downregulation likely reflects reduced iron burden and ferroptotic stress in UA44 (*S. stutzeri*).

Building on this molecular evidence, we next measured functional markers of ferroptosis, including lipid peroxidation, MDA levels, and tissue iron content on Day 3 of adulthood [58]. BODIPY staining revealed UA44 (OP50) exhibited a significant increase in oxidised: non-oxidised lipids ratio (2.99 ± 0.25) compared to BY250 (OP50) (0.24 ± 0.02; $p < 0.0001$) (**Figure 6C**). Similarly, MDA levels were significantly elevated in UA44 (OP50) (1.68 ± 0.20) relative to BY250 (OP50) (0.75 ± 0.11; $p < 0.05$) (**Figure 6D**). In addition, tissue iron content was markedly higher in UA44 (OP50) (1.23 ± 0.18) compared to BY250 (OP50) (0.30 ± 0.21; $p < 0.05$) (**Figure 6E**). Collectively, these results indicate enhanced ferroptosis in the UA44 PD model.

Notably, UA44 (*S. stutzeri*) worms exhibited significantly reduced oxidised: non-oxidised lipids ratio (0.12 ± 0.01; $p < 0.0001$), MDA levels (0.74 ± 0.08; $p < 0.05$), and iron accumulation (0.17 ± 0.09; $p < 0.01$) compared to UA44 (OP50) (**Figure 6C-E**). These results provide strong evidence that *S. stutzeri* mitigates ferroptosis-related oxidative stress, thereby alleviating a key pathogenic process underlying PD-like neurodegeneration.

4. Discussion

Here, we report the neuroprotective effects of *Stutzerimonas stutzeri*, a marine-derived bacterium previously unrecognized for its role in neuroprotection. *S. stutzeri* supplementation conferred robust neuroprotection across multiple PD-relevant phenotypes. In UA44 worms, *S. stutzeri* preserved DA neuron integrity, mitigating hallmark neurodegeneration. Importantly, this structural protection translated into functional rescue: worms fed OP50 showed impaired dopamine-dependent chemotaxis and α-synuclein–linked suppression of pharyngeal pumping, which *S. stutzeri* ameliorated. These results suggest that *S. stutzeri* prevents DA neuron loss and preserves sensory-motor outputs critical for organismal fitness.

α-Synuclein aggregation is a central driver of PD pathogenesis [59]. Using the NL5901 strain, we found that *S. stutzeri* reduced α-synuclein aggregation while decreasing transcript and protein levels. This dual suppression suggests a mechanism that operates upstream at the transcriptional level, reducing the protein pool available for misfolding. Targeting α-synuclein expression is an attractive therapeutic strategy, complementing ongoing approaches aimed at aggregation clearance or immunotherapy [60].

Whole-transcriptome analysis revealed many differentially expressed genes in UA44 worms fed *S. stutzeri*, implicating global reprogramming of proteostasis, stress response, and metabolic networks. Notably, Reactome enrichment highlighted iron uptake and transport, a pathway closely tied to ferroptosis. Ferroptosis, an iron-dependent form of regulated cell death, is increasingly recognized as a driver of PD progression [61,62]. Human studies have demonstrated excess iron deposition in the SNpc correlating with DA neuron loss and impaired striatal function [61,62]. Iron chelators are promising therapies for PD by reducing iron-induced oxidative stress and DA neuron loss. Deferiprone, which crosses the blood-brain barrier, has shown efficacy in phase II trials by lowering iron in the SNpc and improving motor symptoms in early PD [63,64]. Natural polyphenols also provide neuroprotection by binding iron and reducing oxidative damage and α-synuclein aggregation [65]. Consistent with these clinical insights, our transcriptomic analysis revealed that *S. stutzeri* downregulated *ftn-1*, the ferritin heavy chain ortholog, suggesting alleviation of iron burden and ferroptotic stress. To substantiate this interpretation, we assessed biochemical markers of ferroptosis: UA44 (OP50) worms displayed elevated lipid peroxidation, MDA levels, and tissue iron content, all significantly reduced upon *S. stutzeri* supplementation. Although ferritin is often upregulated as a protective response to iron overload, reduced *ftn-1* expression in UA44 (*S. stutzeri*) occurs concomitantly with normalized iron levels and diminished oxidative damage [66,67]. This pattern is consistent with alleviation of iron stress and a reduced requirement for ferritin-mediated iron sequestration following restoration of iron homeostasis, rather than impaired iron buffering. These findings identify *S. stutzeri* as a novel biological intervention that

attenuates ferroptosis-linked stress, thereby safeguarding DA neurons from iron-driven oxidative injury.

Stutzerimonas spp. are versatile bacteria with diverse applications: environmental bioremediation (degrading hydrocarbons, pesticides like chlorpyrifos, and heavy metals); agricultural biotechnology (promoting plant growth, enhancing salt stress tolerance via biofilm formation and nutrient cycling); wastewater treatment (aerobic denitrification, selenium oxyanion reduction); and production of antimicrobial compounds against drug-resistant pathogens [25,26,68-70]. This work establishes *S. stutzeri* as a previously unrecognized marine-derived bacterium with potent neuroprotective activity in *C. elegans* PD models, thereby unveiling an untapped microbial resource with promising neurotherapeutic potential. Marine polysaccharides such as fucoidan from brown algae exhibit antioxidant and anti-inflammatory effects, protecting DA neurons and crossing the blood-brain barrier [71]. Bromophenols sourced from red algae like *Symphyocladia latiuscula* act as multi-target agents, functioning as MAO-A inhibitors and dopamine receptor agonists, thus offering neuroprotection relevant to PD and other neurodegenerative conditions [72]. Within this landscape, *S. stutzeri* represents a new category: a marine bacterium with previously unrecognized neuroprotective activity. Its ability to modulate α-synuclein expression, DA neuron survival, and ferroptosis-associated oxidative stress positions it as a unique therapeutic candidate.

The multifaceted actions of *S. stutzeri*—encompassing DA neuron preservation, behavioral rescue, suppression of α-synuclein, and inhibition of ferroptosis-associated oxidative stress—highlight the value of microbial interventions targeting convergent mechanisms of PD pathology. At the same time, limitations remain*: C. elegans* lacks the complex brain circuitry of mammals, and the precise bacterial factors responsible for neuroprotection remain unidentified. Future studies should aim to isolate *S. stutzeri*-derived metabolites, test efficacy in mammalian PD models, and assess safety and translational feasibility. While our data demonstrate attenuation of iron-dependent lipid peroxidation and oxidative stress, they do not conclusively establish direct inhibition of ferroptotic cell death. Accordingly, our findings are best interpreted as modulation of ferroptosis-associated oxidative stress. The absence of pharmacological validation using a canonical ferroptosis inhibitor such as ferrostatin-1 represents a limitation of the current study. Future studies incorporating genetic or pharmacological ferroptosis modulators will be important to further delineate the contribution of ferroptotic pathways to the neuroprotective effects of *S. stutzeri*.

While this study demonstrates neuroprotection by *S. stutzeri*, we did not perform a comprehensive quantitative assessment of baseline physiological parameters in non-disease control strains, although no overt developmental or behavioral abnormalities were observed. Importantly, the observed effects were phenotype-specific, selectively rescuing DA neuron integrity, dopamine-dependent behaviors, α-synuclein burden, and ferroptosis-associated

molecular markers, rather than broadly enhancing physiological outputs. Together with transcriptomic and biochemical evidence linking *S. stutzeri* to modulation of iron homeostasis and oxidative stress pathways, these findings argue against a nonspecific dietary effect, while highlighting directions for future investigation.

Although *S. stutzeri* demonstrates robust neuroprotective effects in *C. elegans*, we do not currently envision its direct use as a probiotic in humans, given its marine origin and lack of established compatibility with the human gut microbiome. Rather, *S. stutzeri* serves as a valuable biological source for the discovery of neuroactive metabolites or postbiotic factors capable of modulating α-synuclein expression and iron-dependent oxidative stress. Future studies aimed at isolating and characterizing these bacterial-derived factors, followed by validation in mammalian models, will be essential for assessing translational potential.

Collectively, our work identifies *S. stutzeri* as a novel marine-derived bacterium with potent neuroprotective activity. By addressing core pathogenic processes—iron dysregulation, ferroptosis-associated oxidative stress, and α-synuclein accumulation—*S. stutzeri* exemplifies how marine microbes can serve as innovative resources for developing disease-modifying therapies in PD. Given the limitations of current symptomatic treatments and the urgent need for disease-modifying strategies, these findings advance understanding of marine microbe-derived interventions targeting fundamental pathogenic drivers, such as iron dysregulation and ferroptosis-associated oxidative stress.

Abbreviations

PD	Parkinson's disease
DA	Dopaminergic
SNpc	Substantia nigra pars compacta
NGM	Nematode Growth Medium
L1	First larval stage
MDA	Malondialdehyde
DEGs	Differentially Expressed Genes

Keywords

Parkinson's disease, *Stutzerimonas stutzeri*, *Caenorhabditis elegans,* Dopaminergic neurons, Ferroptosis, Iron homeostasis

Data Availability Statement

The datasets generated for the current study are available in the NCBI Gene Expression Omnibus (GEO) repository under accession code GSE312231. The Reviewer Token is uzqbimekrvydlkt for accessing the GEO dataset.

The processed data downloaded from the Galaxy platform after analysis using the LIMMA package is provided in **Supplementary Information 4**.

CRediT Author Contribution Statement

SS- Investigation, Data curation, Validation, Formal analysis, Visualization, Conceptualization, Methodology, Writing – original draft.

AD- Investigation, Data curation, Formal analysis, Visualization, Methodology, Writing – original draft,

SG- Investigation; Data curation; Formal analysis; Visualization, Writing - original draft.

ML- Investigation; Data curation

MP- Resources; Investigation; Methodology; Writing - original draft, Writing - review & editing.

SV- Conceptualization; Investigation; Data curation; Formal analysis; Methodology; Project administration;

Resources; Supervision; Validation; Visualization; Writing - original draft; and Writing - review & editing.

Conflict of Interest

The authors declare no conflict of interest

Declaration of Interest

The authors declare that they have no known competing financial interests or personal relationships that could have appeared to influence the work reported in this paper.

Generative AI statement

While preparing this work, the author(s) used Grammarly to improve language and readability. The author(s) reviewed and edited the content as needed and take(s) full responsibility for the content of the publication.

Acknowledgements

SS is supported by the University Grants Commission, India. AD is supported by the Council of Scientific & Industrial Research, India. SG is supported by the Ministry of Earth Sciences, India. We gratefully acknowledge the Director of CSIR-CDRI for supporting this work by providing the essential research facilities.

Ethics Statement

This study did not require approval from an institutional ethics committee, as it did not involve human participants, animal subjects, or sensitive data.

Funding Statement

The work is supported by in-house funding (IHP0046) from the Director, CSIR-CDRI, to SV.

Highlights

1. Marine bacterium *S. stutzeri* preserves dopaminergic neurons in *C. elegans* Parkinson's disease models.
2. *S. stutzeri* restores dopamine-dependent behaviors in UA44 worms.
3. *S. stutzeri* reduces α-synuclein expression.
4. Induces widespread transcriptomic remodelling; pathway enrichment highlights iron uptake and transport, implicating ferroptosis as a central target of *S. stutzeri*.
5. Downregulates *ftn-1* (ferritin heavy chain ortholog) and significantly reduces lipid peroxidation, malondialdehyde, and iron levels.

References

1 Collaborators, G. B. D. N. Global, regional, and national burden of neurological disorders, 1990-2016: a systematic analysis for the Global Burden of Disease Study 2016. *Lancet Neurol* **18**, 459-480, doi:10.1016/S1474-4422(18)30499-X (2019).

2 Dorsey, E. R., Sherer, T., Okun, M. S. & Bloem, B. R. The Emerging Evidence of the Parkinson Pandemic. *J Parkinsons Dis* **8**, S3-S8, doi:10.3233/JPD-181474 (2018).

3 Shin, H. W., Hong, S. W. & Youn, Y. C. Clinical Aspects of the Differential Diagnosis of Parkinson's Disease and Parkinsonism. *J Clin Neurol* **18**, 259-270, doi:10.3988/jcn.2022.18.3.259 (2022).

4 Asano, H. *et al.* Safety comparisons among monoamine oxidase inhibitors against Parkinson's disease using FDA adverse event reporting system. *Sci Rep* **13**, 19272, doi:10.1038/s41598-023-44142-2 (2023).

5 Pandey, S. & Srivanitchapoom, P. Levodopa-induced Dyskinesia: Clinical Features, Pathophysiology, and Medical Management. *Ann Indian Acad Neurol* **20**, 190-198, doi:10.4103/aian.AIAN_239_17 (2017).

6 Dixon, S. J. *et al.* Ferroptosis: an iron-dependent form of nonapoptotic cell death. *Cell* **149**, 1060-1072, doi:10.1016/j.cell.2012.03.042 (2012).

7 Li, J. *et al.* Ferroptosis: past, present and future. *Cell Death Dis* **11**, 88, doi:10.1038/s41419-020-2298-2 (2020).

8 Dexter, D. T. *et al.* Increased nigral iron content in postmortem parkinsonian brain. *Lancet* **2**, 1219-1220, doi:10.1016/s0140-6736(87)91361-4 (1987).

9 Hirsch, E. C., Brandel, J. P., Galle, P., Javoy-Agid, F. & Agid, Y. Iron and aluminum increase in the substantia nigra of patients with Parkinson's disease: an X-ray microanalysis. *J Neurochem* **56**, 446-451, doi:10.1111/j.1471-4159.1991.tb08170.x (1991).

10 Bellinger, F. P. *et al.* Glutathione Peroxidase 4 is associated with Neuromelanin in Substantia Nigra and Dystrophic Axons in Putamen of Parkinson's brain. *Mol Neurodegener* **6**, 8, doi:10.1186/1750-1326-6-8 (2011).

11 Pearce, R. K., Owen, A., Daniel, S., Jenner, P. & Marsden, C. D. Alterations in the distribution of glutathione in the substantia nigra in Parkinson's disease. *J Neural Transm (Vienna)* **104**, 661-677, doi:10.1007/BF01291884 (1997).

12 Vallerga, C. L. *et al.* Analysis of DNA methylation associates the cystine-glutamate antiporter SLC7A11 with risk of Parkinson's disease. *Nat Commun* **11**, 1238, doi:10.1038/s41467-020-15065-7 (2020).

13 Do Van, B. *et al.* Ferroptosis, a newly characterized form of cell death in Parkinson's disease that is regulated by PKC. *Neurobiol Dis* **94**, 169-178, doi:10.1016/j.nbd.2016.05.011 (2016).

14 Tian, Y. *et al.* FTH1 Inhibits Ferroptosis Through Ferritinophagy in the 6-OHDA Model of Parkinson's Disease. *Neurotherapeutics* **17**, 1796-1812, doi:10.1007/s13311-020-00929-z (2020).

15 Bai, L. *et al.* Thioredoxin-1 Rescues MPP(+)/MPTP-Induced Ferroptosis by Increasing Glutathione Peroxidase 4. *Mol Neurobiol* **58**, 3187-3197, doi:10.1007/s12035-021-02320-1 (2021).

16 Zuo, Y. *et al.* Ferritinophagy-Mediated Ferroptosis Involved in Paraquat-Induced Neurotoxicity of Dopaminergic Neurons: Implication for Neurotoxicity in PD. *Oxid Med Cell Longev* **2021**, 9961628, doi:10.1155/2021/9961628 (2021).

17 Pingale, T. & Gupta, G. L. Classic and evolving animal models in Parkinson's disease. *Pharmacol Biochem Behav* **199**, 173060, doi:10.1016/j.pbb.2020.173060 (2020).

18 Cooper, J. F. & Van Raamsdonk, J. M. Modeling Parkinson's Disease in C. elegans. *J Parkinsons Dis* **8**, 17-32, doi:10.3233/JPD-171258 (2018).

19 Alves, C. *et al.* From Marine Origin to Therapeutics: The Antitumor Potential of Marine Algae-Derived Compounds. *Front Pharmacol* **9**, 777, doi:10.3389/fphar.2018.00777 (2018).

20 El Gamal, A. A. Biological importance of marine algae. *Saudi Pharm J* **18**, 1-25, doi:10.1016/j.jsps.2009.12.001 (2010).

21 Koppula, S. *et al.* Recent advances on the neuroprotective potential of antioxidants in experimental models of Parkinson's disease. *Int J Mol Sci* **13**, 10608-10629, doi:10.3390/ijms130810608 (2012).

22 Mena, M. A. *et al.* NP7 protects from cell death induced by oxidative stress in neuronal and glial midbrain cultures from parkin null mice. *FEBS Lett* **583**, 168-174, doi:10.1016/j.febslet.2008.11.051 (2009).

23 Lee, H. W., Choi, H., Nam, S. J., Fenical, W. & Kim, H. Potent Inhibition of Monoamine Oxidase B by a Piloquinone from Marine-Derived Streptomyces sp. CNQ-027. *J Microbiol Biotechnol* **27**, 785-790, doi:10.4014/jmb.1612.12025 (2017).

24 Silva, J. *et al.* Marine-Derived Components: Can They Be a Potential Therapeutic Approach to Parkinson's Disease? *Mar Drugs* **21**, doi:10.3390/md21080451 (2023).

25 Lenchi, N., Ahmedi, W. & Kebbouche-Gana, S. Assessment of bioremediation potential of Stutzerimonas stutzeri NL3 and Enterobacter cloacae NL4 isolates from an Algerian oilfield. *Environ Technol* **46**, 3168-3184, doi:10.1080/09593330.2025.2458796 (2025).

26 Li, L. *et al.* Stutzerimonas stutzeri culture enhances microbial community structure and tomato seedling growth in saline soil. *J Appl Microbiol* **136**, doi:10.1093/jambio/lxaf026 (2025).

27 Tripathi, V. C. *et al.* The discovery of antioxidants in marine microorganisms and their protective effects on the hepatic cells from chemical-induced oxidative stress. *Free Radic Res* **54**, 150-161, doi:10.1080/10715762.2020.1725499 (2020).

28 Assembler & Baser Sequence, D. N. A. v3. x (2012) Heracle BioSoft SRL Romania. *Available: Accessed(30)* (2012).

29 Wright, E. S., Yilmaz, L. S. & Noguera, D. R. DECIPHER, a search-based approach to chimera identification for 16S rRNA sequences. *Applied and environmental microbiology* **78**, 717-725 (2012).

30 Brenner, S. The genetics of Caenorhabditis elegans. *Genetics* **77**, 71-94, doi:10.1093/genetics/77.1.71 (1974).

31 Manalo, R. V. M. & Medina, P. M. B. Caffeine reduces deficits in mechanosensation and locomotion induced by L-DOPA and protects dopaminergic neurons in a transgenic Caenorhabditis elegans model of Parkinson's disease. *Pharm Biol* **58**, 721-731, doi:10.1080/13880209.2020.1791192 (2020).

32 Zhang, Z. *et al.* Jujubae Fructus extract prolongs lifespan and improves stress tolerance in Caenorhabditis elegans dependent on DAF-16/SOD-3. *Sci Rep* **14**, 13713, doi:10.1038/s41598-024-64045-0 (2024).

33 Promtang, S. *et al.* 2-Butoxytetrahydrofuran, Isolated from Holothuria scabra, Attenuates Aggregative and Oxidative Properties of alpha-Synuclein and Alleviates Its Toxicity in a Transgenic Caenorhabditis elegans Model of Parkinson's Disease. *ACS Chem Neurosci* **15**, 2182-2197, doi:10.1021/acschemneuro.4c00008 (2024).

34 Zhu, F. D. *et al.* Carpesii fructus extract exhibits neuroprotective effects in cellular and Caenorhabditis elegans models of Parkinson's disease. *CNS Neurosci Ther* **30**, e14515, doi:10.1111/cns.14515 (2024).

35 Verma, S., Jagtap, U., Goyala, A. & Mukhopadhyay, A. A novel gene-diet pair modulates C. elegans aging. *PLoS Genet* **14**, e1007608, doi:10.1371/journal.pgen.1007608 (2018).

36 Murayama, T. & Maruyama, I. N. Plate Assay to Determine Caenorhabditis elegans Response to Water Soluble and Volatile Chemicals. *Bio Protoc* **8**, e2740, doi:10.21769/BioProtoc.2740 (2018).

37 Sammi, S. R., Syeda, T., Conrow, K. D., Leung, M. C. K. & Cannon, J. R. Complementary biological and computational approaches identify distinct mechanisms of chlorpyrifos versus chlorpyrifos-oxon-induced dopaminergic neurotoxicity. *Toxicol Sci* **191**, 163-178, doi:10.1093/toxsci/kfac114 (2023).

38 Yong, Y. Y. *et al.* Penthorum chinense Pursh inhibits ferroptosis in cellular and Caenorhabditis elegans models of Alzheimer's disease. *Phytomedicine* **127**, 155463, doi:10.1016/j.phymed.2024.155463 (2024).

39 Ko, B. & Van Raamsdonk, J. M. RNA Sequencing of Pooled Samples Effectively Identifies Differentially Expressed Genes. *Biology (Basel)* **12**, doi:10.3390/biology12060812 (2023).

40 Takele Assefa, A., Vandesompele, J. & Thas, O. On the utility of RNA sample pooling to optimize cost and statistical power in RNA sequencing experiments. *BMC Genomics* **21**, 312, doi:10.1186/s12864-020-6721-y (2020).

41 Cheng, C. *et al.* Multiplexed bulk and single-cell RNA-seq hybrid enables cost-efficient disease modeling with chimeric organoids. *Nat Commun* **15**, 3946, doi:10.1038/s41467-024-48282-5 (2024).

42 Everett, L. J. *et al.* Gene expression networks in the Drosophila Genetic Reference Panel. *Genome Res* **30**, 485-496, doi:10.1101/gr.257592.119 (2020).

43 Galaxy, C. The Galaxy platform for accessible, reproducible, and collaborative data analyses: 2024 update. *Nucleic Acids Res* **52**, W83-W94, doi:10.1093/nar/gkae410 (2024).

44 Dennis, G., Jr. *et al.* DAVID: Database for Annotation, Visualization, and Integrated Discovery. *Genome Biol* **4**, P3 (2003).

45 Kolberg, L., Raudvere, U., Kuzmin, I., Vilo, J. & Peterson, H. gprofiler2 -- an R package for gene list functional enrichment analysis and namespace conversion toolset g:Profiler. *F1000Res* **9**, doi:10.12688/f1000research.24956.2 (2020).

46 Rahman, A. *et al.* Whole genome sequence of denitrifying bacterium Stutzerimonas stutzeri strain NGHE31, collected from an eutrophic wetland in Sunamganj, Bangladesh, following the 2017 flash floods. *Microbiol Resour Announc* **13**, e0000124, doi:10.1128/mra.00001-24 (2024).

47 Gomila, M., Mulet, M., Garcia-Valdes, E. & Lalucat, J. Genome-Based Taxonomy of the Genus Stutzerimonas and Proposal of S. frequens sp. nov. and S. degradans sp. nov. and Emended Descriptions of S. perfectomarina and S. chloritidismutans. *Microorganisms* **10**, doi:10.3390/microorganisms10071363 (2022).

48 Gaeta, A. L., Caldwell, K. A. & Caldwell, G. A. Found in Translation: The Utility of C. elegans Alpha-Synuclein Models of Parkinson's Disease. *Brain Sci* **9**, doi:10.3390/brainsci9040073 (2019).

49 Felton, C. M. & Johnson, C. M. Dopamine signaling in C. elegans is mediated in part by HLH-17-dependent regulation of extracellular dopamine levels. *G3 (Bethesda)* **4**, 1081-1089, doi:10.1534/g3.114.010819 (2014).

50 Ward, S. Chemotaxis by the nematode Caenorhabditis elegans: identification of attractants and analysis of the response by use of mutants. *Proc Natl Acad Sci U S A* **70**, 817-821, doi:10.1073/pnas.70.3.817 (1973).

51 Bargmann, C. I., Hartwieg, E. & Horvitz, H. R. Odorant-selective genes and neurons mediate olfaction in C. elegans. *Cell* **74**, 515-527, doi:10.1016/0092-8674(93)80053-h (1993).

52 Kaur, S., Sammi, S. R., Jadiya, P. & Nazir, A. RNAi of cat-2, a putative tyrosine hydroxylase, increases alpha synuclein aggregation and associated effects in transgenic C. elegans. *CNS Neurol Disord Drug Targets* **11**, 387-394, doi:10.2174/187152712800792811 (2012).

53 Muhammad, F. *et al.* Neuroprotective effects of cannabidiol on dopaminergic neurodegeneration and alpha-synuclein accumulation in C. elegans models of Parkinson's disease. *Neurotoxicology* **93**, 128-139, doi:10.1016/j.neuro.2022.09.001 (2022).

54 Sherman, D. & Harel, D. Deciphering the underlying mechanisms of the pharyngeal pumping motions in Caenorhabditis elegans. *Proc Natl Acad Sci U S A* **121**, e2302660121, doi:10.1073/pnas.2302660121 (2024).

55 Maulik, M., Mitra, S., Bult-Ito, A., Taylor, B. E. & Vayndorf, E. M. Behavioral Phenotyping and Pathological Indicators of Parkinson's Disease in C. elegans Models. *Front Genet* **8**, 77, doi:10.3389/fgene.2017.00077 (2017).

56 Ayton, S. & Lei, P. Nigral iron elevation is an invariable feature of Parkinson's disease and is a sufficient cause of neurodegeneration. *Biomed Res Int* **2014**, 581256, doi:10.1155/2014/581256 (2014).

57 He, N. *et al.* Increased iron-deposition in lateral-ventral substantia nigra pars compacta: A promising neuroimaging marker for Parkinson's disease. *Neuroimage Clin* **28**, 102391, doi:10.1016/j.nicl.2020.102391 (2020).

58 Sun, D. *et al.* Lipid metabolism in ferroptosis: mechanistic insights and therapeutic potential. *Front Immunol* **16**, 1545339, doi:10.3389/fimmu.2025.1545339 (2025).

59 Srinivasan, E. *et al.* Alpha-Synuclein Aggregation in Parkinson's Disease. *Front Med (Lausanne)* **8**, 736978, doi:10.3389/fmed.2021.736978 (2021).

60 Teil, M. *et al.* Targeting alpha-synuclein for PD Therapeutics: A Pursuit on All Fronts. *Biomolecules* **10**, doi:10.3390/biom10030391 (2020).

61 Yao, Z. *et al.* Ferroptosis in Parkinson's disease -- The iron-related degenerative disease. *Ageing Res Rev* **101**, 102477, doi:10.1016/j.arr.2024.102477 (2024).

62 Zhou, M. *et al.* Targeting Ferroptosis in Parkinson's Disease: Mechanisms and Emerging Therapeutic Strategies. *Int J Mol Sci* **25**, doi:10.3390/ijms252313042 (2024).

63 Devos, D. *et al.* Therapeutic modalities of deferiprone in Parkinson's disease: SKY and EMBARK studies. *J Parkinsons Dis* **15**, 72-86, doi:10.1177/1877718X241300295 (2025).

64 Zeng, W., Cai, J., Zhang, L. & Peng, Q. Iron Deposition in Parkinson's Disease: A Mini-Review. *Cell Mol Neurobiol* **44**, 26, doi:10.1007/s10571-024-01459-4 (2024).

65 Chen, Y. *et al.* The interplay of iron, oxidative stress, and alpha-synuclein in Parkinson's disease progression. *Mol Med* **31**, 154, doi:10.1186/s10020-025-01208-3 (2025).

66 Chen, Z. T. *et al.* Evaluation of ferritin and TfR level in plasma neural-derived exosomes as potential markers of Parkinson's disease. *Front Aging Neurosci* **15**, 1216905, doi:10.3389/fnagi.2023.1216905 (2023).

67 Friedman, A. & Galazka-Friedman, J. The history of the research of iron in parkinsonian substantia nigra. *J Neural Transm (Vienna)* **119**, 1507-1510, doi:10.1007/s00702-012-0894-8 (2012).

68 Perez-Padilla, V., Molina-Henares, M. A., Udaondo, Z., Ramos-Gonzalez, M. I. & Espinosa-Urgel, M. Genetic basis of biofilm formation and salt adaptation in the plant-beneficial strain Stutzerimonas stutzeri MJL19. *Appl Microbiol Biotechnol* **109**, 130, doi:10.1007/s00253-025-13523-0 (2025).

69 Zhang, B. *et al.* Unlocking N(2)O respiratory pathways in Stutzerimonas stutzeri PRE-2: Implications for reducing N(2)O emissions from estuaries. *Mar Environ Res* **206**, 107044, doi:10.1016/j.marenvres.2025.107044 (2025).

70 Devkar, H. U. *et al.* Antimicrobial Potential of Marine Sponge-Associated Bacillus velezensis and Stutzerimonas stutzeri from the Indian Coast: A Genome Mining and Metabolite Profiling Approach. *Curr Microbiol* **82**, 280, doi:10.1007/s00284-025-04262-6 (2025).

71 Han, M. *et al.* Fucoidan-derived carbon dots as nanopenetrants of blood-brain barrier for Parkinson's disease treatment. *J Colloid Interface Sci* **680**, 516-527, doi:10.1016/j.jcis.2024.10.173 (2025).

72 Paudel, P., Park, S. E., Seong, S. H., Jung, H. A. & Choi, J. S. Bromophenols from Symphyocladia latiuscula Target Human Monoamine Oxidase and Dopaminergic Receptors for the Management of Neurodegenerative Diseases. *J Agric Food Chem* **68**, 2426-2436, doi:10.1021/acs.jafc.0c00007 (2020).

Table 1: Details of Primers used in the study:

Target	Primer	Sequence
	27F	AGAGTTTGATCMTGGCTCAG
	1387R	GGGCGGWGTGTACAAGGC
	63F	CAGGCCTAACACATGCAAGTC
	1525R	AGGAGGTGWTCCARCC
Ftn-1	Forward	AGAACATTCAGAAGCCAGAG
	Reverse	GATCGAATGTACCTGCTCTTC
α-synuclein	Forward	GACAAAAGAGGGTGTTCTCT
	Reverse	GACAAAGCCAGTGGCTGC
β-actin	Forward	GCTGGACGTGATCTTACTGATTACC
	Reverse	GTAGCAGAGCTTCTCCTTGATGTC

Graphical Abstract

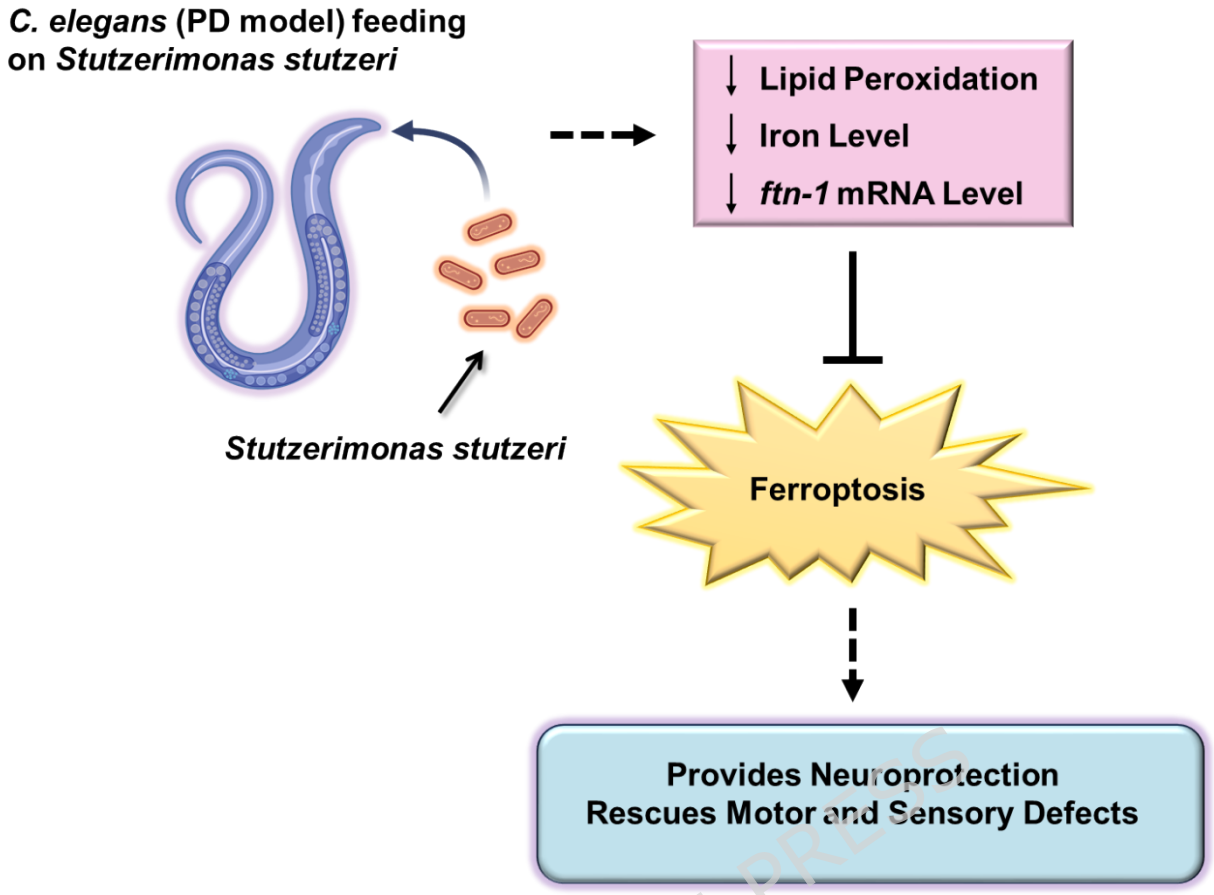

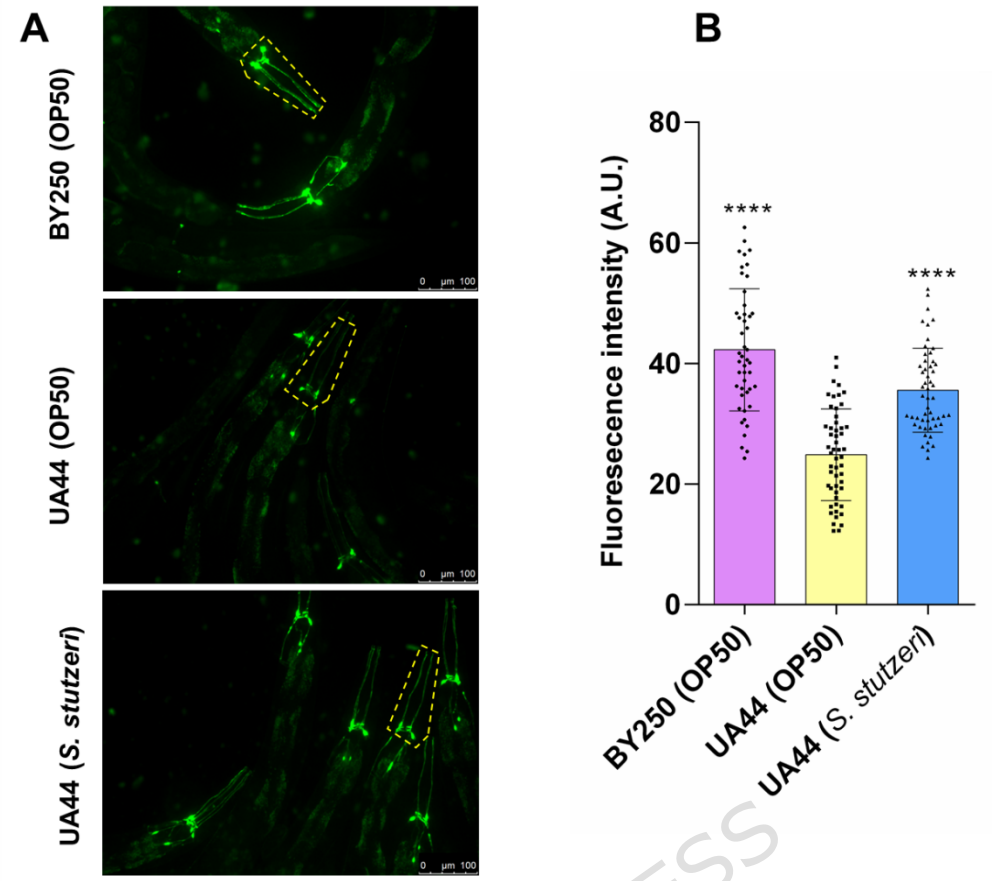

Figure 1. *S. stutzeri* preserves dopaminergic neurons in the *C. elegans* PD model.

(A) Representative fluorescence micrographs of dopaminergic (DA) neurons in the head region of day 3 adult worms from control strain BY250 (OP50), PD model strain UA44 (OP50), and UA44 fed with *S. stutzeri*. The indicated region (yellow dashed lines) outlines the head area used for fluorescence quantification, which includes dopaminergic neuronal cell bodies and their dendritic processes, and reflects the combined signal from these structures. BY250 worms show intact DA neurons, whereas UA44 (OP50) worms exhibit pronounced DA neurodegeneration. UA44 (*S. stutzeri*) worms display preserved DA neuronal morphology. Magnification = 20X.

(B) Quantification of DA neuronal fluorescence intensity by ImageJ. UA44 (OP50) worms showed a significant reduction compared to BY250 (OP50), confirming DA neurodegeneration in the PD model. Supplementation with *S. stutzeri* significantly restored DA neuronal fluorescence intensity in UA44 worms. n ≥ 40 worms (pooled from at least three independent biological replicates).

Data are presented as mean ± SD; ****$p < 0.0001$ compared to UA44 (OP50).

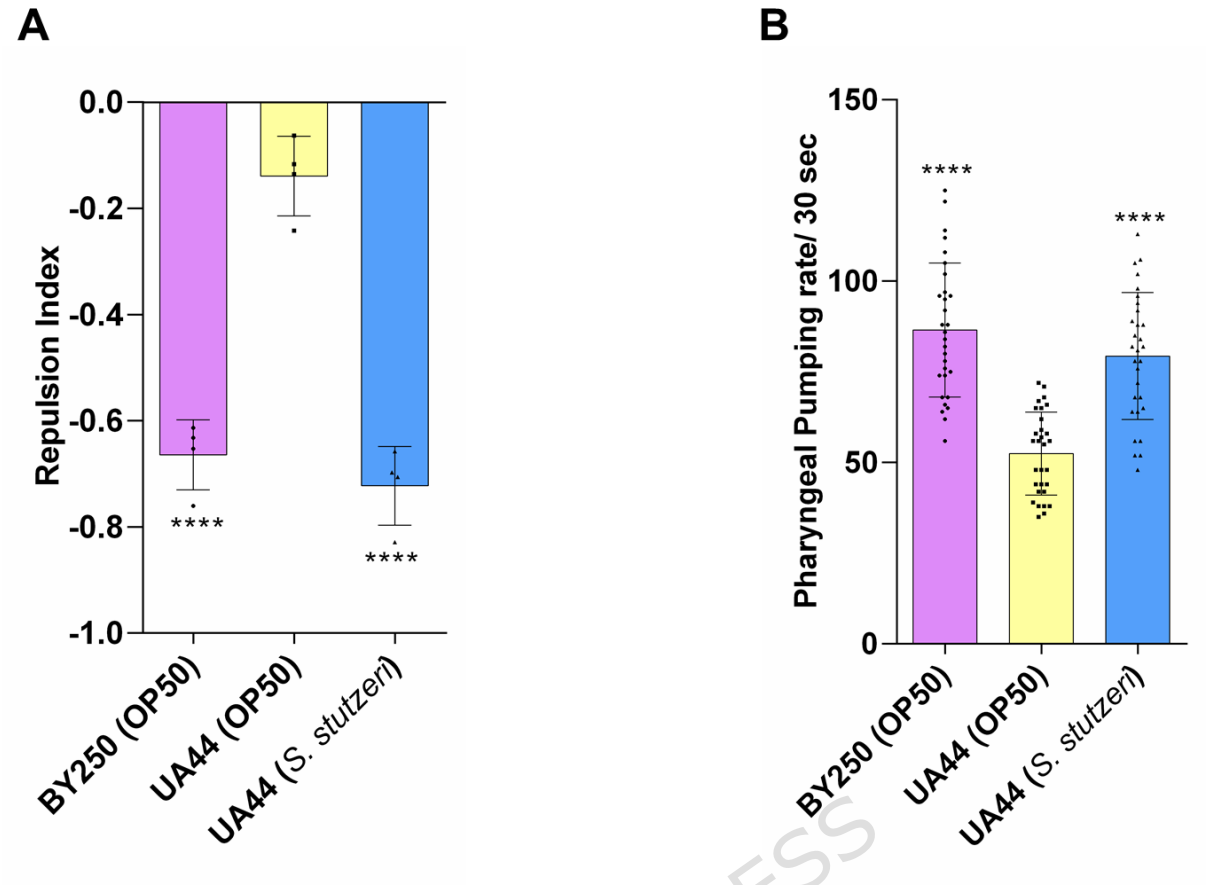

Figure 2. *S. stutzeri* rescues dopamine-dependent chemotaxis and pharyngeal pumping deficits in the *C. elegans* PD model.

(A) Repulsion index in the 1-nonanol avoidance assay. UA44 (OP50) worms displayed a significantly reduced aversive response compared to BY250 (OP50), consistent with impaired dopamine-dependent chemotaxis. Feeding UA44 worms with *S. stutzeri* significantly improved the repulsion index, indicating restoration of dopamine-associated behavior. n=4 biological repeats with ≥30 worms per repeat.

(B) Quantification of pharyngeal pumping rate (contractions per 30 s). UA44 (OP50) worms exhibited a significant reduction in pumping rate compared to BY250 (OP50), validating neuromuscular dysfunction associated with α-synuclein toxicity. *S. stutzeri* supplementation significantly restored pharyngeal pumping in UA44 worms. n ≥ 40 worms (pooled from at least three independent biological replicates).

Data are presented as mean ± SD; ***$p < 0.001$, ****$p < 0.0001$, compared to UA44 (OP50).

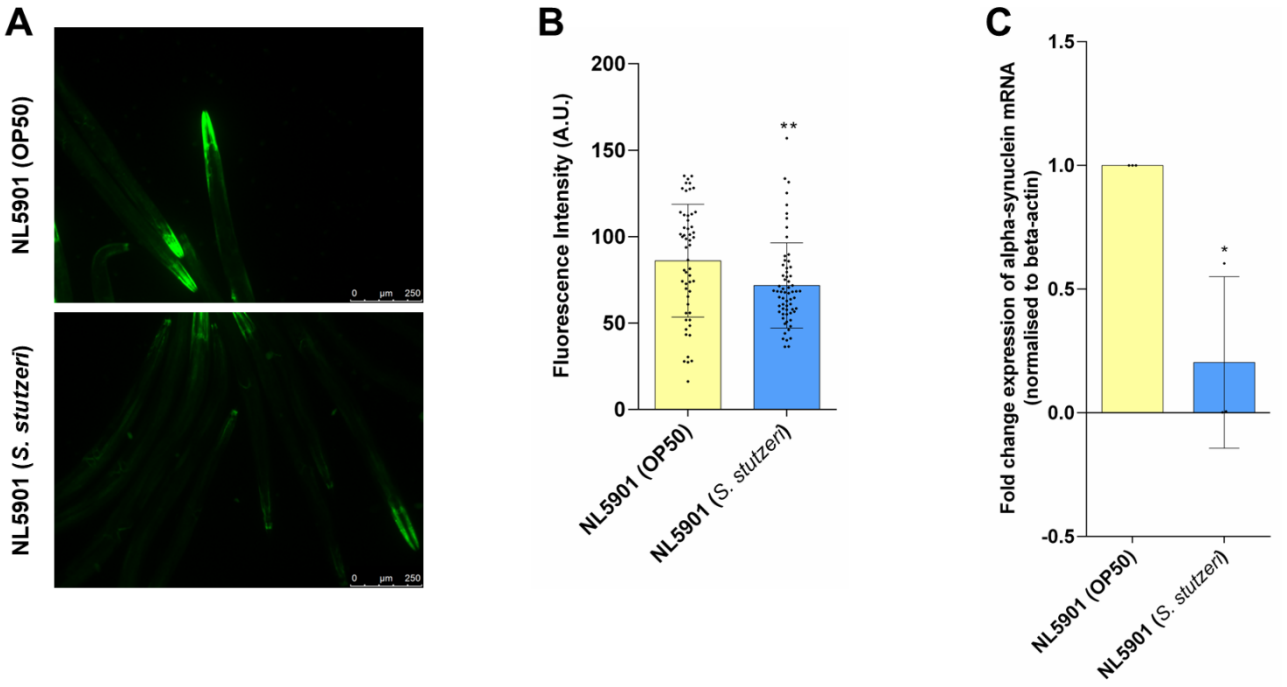

Figure 3. *S. stutzeri* reduces α-synuclein expression in the NL5901 *C. elegans* PD model.

(A) Representative fluorescence micrographs of NL5901 worms expressing human α-synuclein::YFP in body-wall muscle, showing increased fluorescence in worms fed OP50 compared to those fed *S. stutzeri*. Magnification=10X.

(B) Quantification of α-synuclein::YFP fluorescence intensity. NL5901 (OP50) worms displayed significantly elevated expression compared to NL5901 (*S. stutzeri*) worms, which exhibited reduced fluorescence intensity, indicating suppression of α-synuclein accumulation. n ≥ 40 worms (pooled from at least three independent biological replicates).

(C) qRT-PCR analysis of α-synuclein transcript levels normalized to β-actin. NL5901 worms fed with *S. stutzeri* showed a significant reduction in α-synuclein mRNA expression compared to OP50-fed controls. n=3 biological repeats with ≥500 worms per condition per repeat.

Data are presented as mean ± SD; *$p < 0.05$, **$p < 0.01$ compared to NL5901 (OP50).

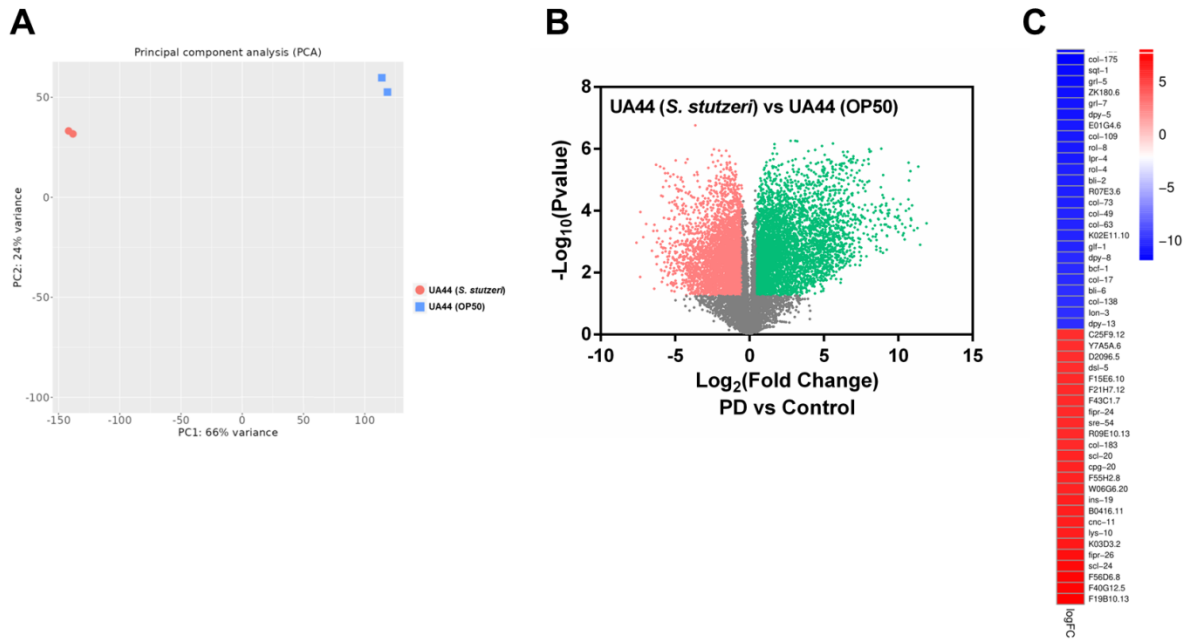

Figure 4. Transcriptomic reprogramming induced by *S. stutzeri* in the UA44 PD model.

(A) Principal component analysis of RNA-seq data showing clear segregation between UA44 worms fed OP50 and UA44 worms fed *S. stutzeri*, indicating distinct global transcriptional profiles.

(B) Volcano plot depicting differentially expressed genes between UA44 (*S. stutzeri*) and UA44 (OP50). A total of 11,950 DEGs were identified ($p \leq 0.05$, $|\log_2$ fold-change$| \geq 0.5$), including 6,138 upregulated (green) and 5,812 downregulated (red) genes in UA44 (*S. stutzeri*).

(C) Heatmap of the top 50 DEGs illustrating distinct transcriptional signatures between UA44 (OP50) and UA44 (*S. stutzeri*). Color scale represents $\log_2$ fold-change values, with red indicating downregulation and blue indicating upregulation.

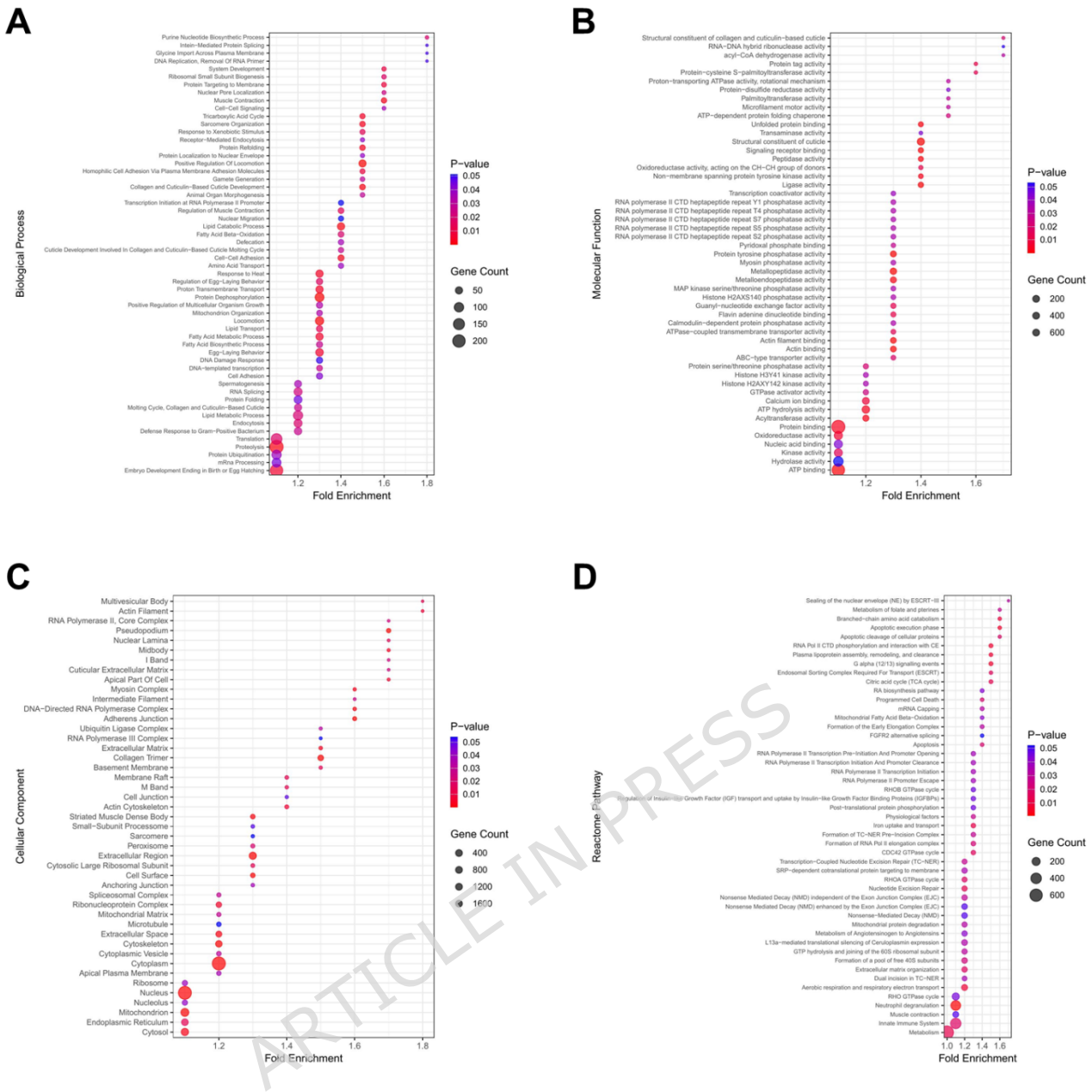

Figure 5. Gene Ontology (GO) and Reactome pathway enrichment analysis of the differentially expressed genes using online software, DAVID. Bubble plots showing the significant GO terms for (A) Biological Processes, (B) Molecular Function, (C) Cellular Component, and (D) Reactome pathway enrichment.

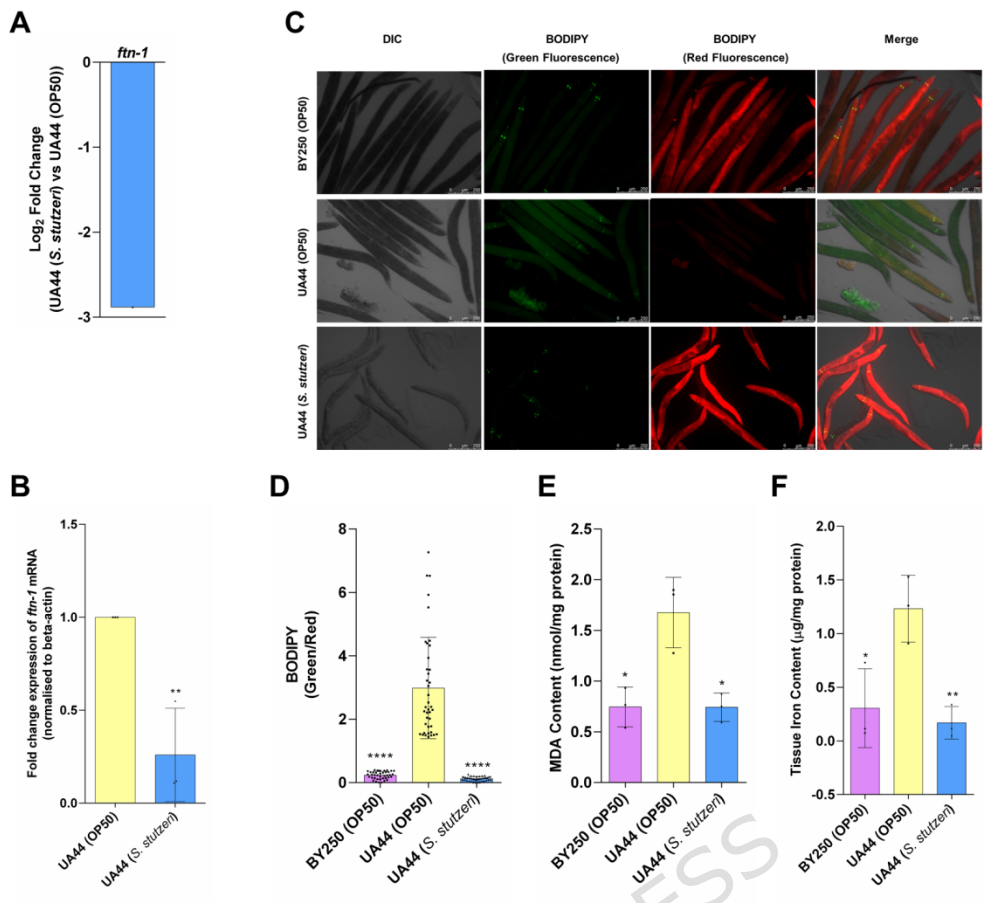

Figure 6. *S. stutzeri* attenuates ferroptosis-related markers in the UA44 PD model.

(A) Transcriptomic analysis revealed significant downregulation of *ftn-1* (ferritin heavy chain ortholog) in UA44 worms fed *S. stutzeri* compared to UA44 (OP50).

(B) qRT-PCR validation confirmed reduced *ftn-1* transcript levels in UA44 (*S. stutzeri*) relative to UA44 (OP50), normalized to β-actin. n=3 biological repeats with ≥500 worms per condition per repeat.

(C) Representative BODIPY staining images showing oxidised lipids (green fluorescence), non-oxidised lipids (red fluorescence), and merged images. UA44 (OP50) worms displayed pronounced lipid peroxidation, which was markedly reduced in UA44 (*S. stutzeri*). Magnification=10X.

(D) Quantification of BODIPY green/red fluorescence ratio confirmed reduced lipid peroxidation in UA44 (*S. stutzeri*) compared to UA44 (OP50). n ≥ 40 worms (pooled from at least three independent biological replicates).

(E) Measurement of malondialdehyde levels, an end product of lipid peroxidation, showed significant elevation in UA44 (OP50) compared to BY250, which was significantly reduced in UA44 (*S. stutzeri*). n=3 biological repeats with ≥500 worms per condition per repeat.

(F) Tissue iron content was significantly higher in UA44 (OP50) than BY250, while *S. stutzeri* supplementation restored iron levels toward control values. n=3 biological repeats with ≥500 worms per condition per repeat.

Data are presented as mean ± SD; *$p < 0.05$, **$p < 0.01$, ****$p < 0.0001$ compared to UA44 (OP50).